SIMULTANEOUSLY EFFECTS OF ELECTRIC AND MAGNETIC FIELDS ON THE DONOR POLARIZABILITY IN GaAs SPHERICAL QUANTUM DOTS

Liliana M. BURILEANU[1], Gabriela C. TIRIBA[2]

The simultaneous effects of the applied electric and magnetic fields on the binding energy and polarizability of a donor impurity in spherical GaAs quantum dots with parabolic confinement are investigated by using the variational procedure, within the effective mass approximation. The results are reported for two different quantum dot radii and different positions of the impurity inside the quantum dot. Our results show that spherical dot impurity binding energy and the polarizability can be tuned by means of the applied external electric and/or magnetic field, which can be used in the semiconductor device design.

Keywords: Polarizability; quantum dot; hydrogen like impurity; electric and magnetic fields.

1. Introduction

In recent years, the quantum dot-like nanostructures have led to an unprecedented development of optoelectronic devices such as infrared photodetectors [1], quantum dot lasers [2], single photon sources [3], single electron transistors [4], solar cells [5], and light emitting diodes [6].

There is also a special interest on the impurity atoms that are added to heterostructures because they significantly increase the number of charge carriers modifying the properties of the host material. The presence of a hydrogenic impurity in a semiconductor nanostructure allow us to change its electronic and optical properties, such as donor binding energy, electronic structure, photoionization cross section, and second-order optical nonlinear properties. In addition there are studies of the influence of external electric and magnetic fields applied on these heterostructures because such fields change the confining potential of the charge carriers and can provide valuable information about the hydrogenic impurity states. There are many articles [7-38] dealing with these topics.

The subject of the impurity polarizability is treated in some of them. Morales et al. evaluated the shallow-impurity polarizability in asymmetric GaAs/GaAlAs double quantum wells under electric field and hydrostatic pressure [25]. Peter

[1] Reader, Physics Department, University Politehnica of Bucharest, Romania, email: burileanu@physics.pub.ro

[2] Reader, Physics Department, University Politehnica of Bucharest, Romania

investigated the effect of electric and magnetic fields on the donor binding energies and polarizability of an on-center shallow donor in finite-barrier GaAs/AlGaAs nanodots [26] and in $Cd_{xin}Mn_{1-xin}Te/Cd_{xout}Mn_{1-xout}Te$ spherical quantum dots (the effect of the electric field only) [27].
The binding energy and the polarizability of a donor impurity in double quantum-well wires under the action of the hydrostatic pressure and applied electric field were studied by Tangarife and Duque. They found a strong dependence of these quantities on the confinement potential and the applied electric field direction [28-29]. Khordad et al. [30] calculated the polarizability of a hydrogenic donor impurity in a ridge quantum wire. Their conclusion was that the binding energy and the polarizability of the impurity strongly depended on the confinement potential, the impurity position and the electric field direction.
The effect of an applied electric field on the binding energy and polarizability of a donor impurity in a prism-shaped GaAs quantum dot with triangular cross-section was theoretically investigated by Cristea and Niculescu [31]. Their study shows that an electric field applied along the dot axis strongly changes the spatial distribution of the electron wave functions, the subsequent energy levels and the donor polarizability.
Satori et al. [32] studied the influence of an applied electric field on the ground state binding energy and the polarizability of a hydrogenic impurity located at the center of a spherical quantum dot with both infinite and finite height confinement potentials.
In this paper we present our studies about the polarizability of a hydrogenic impurity located in a GaAs/AlGaAs spherical quantum dot under joint action of electric and magnetic fields. Calculations are made within the effective mass approximation by using a variational procedure for some dot radii and different positions of the impurity inside the dot. Compared to similar papers previously published we study the electron probability density in the absence/presence of the impurity as a function of the applied fields. Then these results are used to explain the polarizability behavior of this nanostructure. We show that, the binding energy and the polarizability are modified by the applied electric and magnetic fields.

2. Theory

We consider a $GaAs/Ga_{0.7}Al_{0.3}As$ spherical QD and an inside hydrogenic donor impurity under the combined action of static electric and magnetic fields. We assign the reference frame origin to be in the dot center, and consider that the impurity may have any position on the *Oz* axis inside the dot. We choose the applied fields to point toward the negative *z*-axis.

The quantum system acquires cylindrical symmetry and the electron position is denoted by the vector $\vec{r}(\rho,\varphi,z)$. The form of confinement potential of the electron is:

$$V_{conf}(\rho,\varphi,z)=\frac{1}{2}m*\omega_0^2 r^2, \tag{1}$$

where $m*$ is the electron effective mass, $\omega_0=\frac{\hbar}{m*R^2}$ is the frequency of confinement potential for spherical QD of radius R and $r^2=\rho^2+z^2$.

In the effective mass approximation, when the electron is subject to the electric and magnetic field action, the electron Hamiltonian has the general form:

$$\hat{H}=\frac{1}{2m*}\left(\vec{p}+e\vec{A}\right)^2+V_{\text{conf}}+V_{el}+V_{\text{Coulomb}}. \tag{2}$$

In order to exactly solve the corresponding Schrödinger equation we drop the Coulomb energy term for moment and write this reduced Hamiltonian in cylindrical coordinates:

$$\hat{H}^*=-\frac{\hbar^2}{2m*}\left[\frac{1}{\rho}\frac{\partial}{\partial\rho}\left(\rho\frac{\partial}{\partial\rho}\right)+\frac{1}{\rho^2}\frac{\partial^2}{\partial\varphi^2}+\frac{\partial^2}{\partial z^2}\right]-\frac{1}{2}\omega_c\hat{l}_z+\frac{m*\omega_0^2z^2}{2}+\frac{m*\Omega^2\rho^2}{8}-eFz. \tag{3}$$

Here $\hat{l}_z$ is the z-component of the angular momentum operator, e is the elementary charge, F is the electrostatic field strength, $\Omega=\sqrt{\omega_c^2+4\omega_0^2}$ where $\omega_c=\frac{eB}{m*}$ is the cyclotron frequency, and B is the magnetic field strength.

The solution of the $\hat{H}^*$ corresponding Schrödinger eigenvalue equation can be written as $\psi(\rho,\varphi,z)=f(\rho,\varphi)\chi(z)$ and these two functions are [39, 40]:

$$f_{n,m}(\rho,\varphi)=\frac{1}{s^{1+|m|}}\sqrt{\frac{(|m|+n)!}{2\pi 2^{|m|}n!|m|!}}\left(\exp[im\varphi]\right)\cdot\left(\exp[-\frac{\rho^2}{4s^2}]\right)\rho^{|m|}\cdot\mathcal{F}\left(-n,|m|+1;\frac{\rho^2}{2s^2}\right) \tag{4}$$

and

$$\chi_{n_z}(z)=\left(\frac{m*\omega_0}{\pi\hbar}\right)^{\frac{1}{4}}\frac{1}{\sqrt{2^{n_z}n_z!}}\left(\exp\left[-\frac{m*\omega_0}{2\hbar}\left(z-\frac{eF}{m*\omega_0^2}\right)^2\right]\right)\times$$
$$\times H_{n_z}\left[\sqrt{\frac{m*\omega_0}{\hbar}}\left(z-\frac{eF}{m*\omega_0^2}\right)\right]. \tag{5}$$

In Eqs. (4) and (5) $s=\sqrt{\hbar/m^*\Omega}$, $F(a,b;x)$ is the confluent hypergeometric function, n is the radial quantum number, m is the magnetic quantum number, $H_{n_z}(z)$ is the Hermite polynomial and n_z is the harmonic quantum number.

The electron eigenenergies are given by

$$E_{n,m,n_z}=\hbar\Omega\left(n+\frac{1+|m|}{2}\right)-\frac{m\hbar\omega_c}{2}+\hbar\omega_0\left(n_z+\frac{1}{2}\right)-\frac{e^2F^2}{2m^*\omega_0^2}. \tag{6}$$

In what follows we will only refer to the ground state of the electron whose wave function and energy are denoted by ϕ_0 and E_0 respectively.

In the presence of the impurity the Hamiltonian given by Eq. (3) must be completed with the Coulomb energy term $-\frac{e^2}{4\pi\varepsilon}\cdot\frac{1}{|\vec{r}-\vec{r}_i|}$, depending on the impurity position $\vec{r}_i(0,0,z_i)$. The eigenvalues of this Hamiltonian $\hat{H}$ cannot be exactly found so that an approximate method should be used. We apply the variational method using the following trial functions [28]:

$$\Phi_\lambda(\rho,\varphi,z;z_i)=\phi_0(\rho,\varphi,z)\exp[-\lambda(|\vec{r}-\vec{r}_i|)], \tag{7}$$

where λ is the variational parameter depending on *F*, *B*, and z_i.

We obtain the minimum energy of the electron in the presence of the impurity and the applied fields namely the ground state energy of the complete system:

$$E_{\min}=\min_\lambda\frac{\langle W|\hat{H}|W\rangle}{\langle W|W\rangle} \tag{8}$$

and the electron binding energy as the difference between the ground-state energy without impurity and this minimum energy

$$E_b=E_0-E_{\min}, \tag{9}$$

where for short, $W\equiv\Phi_\lambda(\rho,\varphi,z;z_i)$.

This new ground state wave function *W* may be also used to calculate the dot polarizability due to the applied fields in the impurity presence.

The electron cloud electric moment due to the applied fields is defined as [26]:

$$P=\langle -ez\rangle_{F\neq0}-\langle -ez\rangle_{F=0}=\alpha_p\cdot(-F) \tag{10}$$

so that the dot polarizability α_p is [25, 28-31, 41]:

$$\alpha_p=\frac{e}{F}\left[\langle W|z|W\rangle_{F\neq0}-\langle W|z|W\rangle_{F=0}\right]. \tag{11}$$

3. Results and discussion

In what follows, the required parameters used in our calculations are [42]: $m^* = 0.0665 m_0$, and $\varepsilon_r = 12.4$.

The effect of the electric and magnetic fields on the electron cloud localization in the absence of the impurity is shown in the Figs. 1 and 2.

Fig. 1 shows the cross section of the probability density in $z = 0$ plane (denoted as *xOy* plane) for the electron ground level under different strengths of applied magnetic field. The results for $R = 8$ nm and $R = 10$ nm are presented in the left panel and the right panel, respectively. The circles drawn with dashed line represent the QD boundary.

In the absence of any applied field (Figs. 1(a) and (c)) the wave function is largely confined around $\vec{r} = 0$, but with increasing QD size the confinement potential overall decreases as the fourth power of its radius.

The effect of the magnetic field (Fig. 1(b) and (d)) on the electron density distribution in the absence of the electric field consists in a stronger confinement of the wave function around the center of the QD compared with the state without applied field.

Changing the observation plane, from *xOy* to *xOz*, the effects of applied fields can be better revealed (Fig. 2). As the electric field strength increases (Figs. 2(a) and (c)) a shift of the electron oscillation center in the opposite field direction occurs but the electron cloud spherical symmetry is preserved. The shift is larger for bigger QD radius at given field strength.

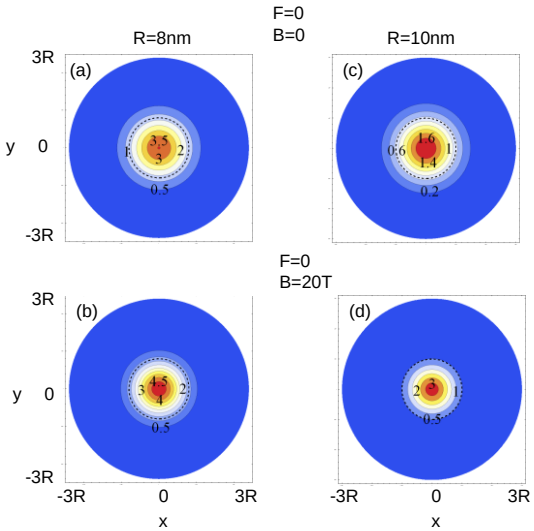

Fig. 1. (Color online) The cross section of the electron probability density for the ground level of spherical GaAs QD without impurity under different strengths of the applied magnetic field directed along the negative *z*-axis. The observation plane is *xOy*. The left panel is for $R = 8$ nm, and the right panel for $R = 10$ nm. The circles drawn with dashed line represent the QDs boundary.

The presence of the magnetic field reduces the spherical symmetry to an ellipsoidal symmetry (Fig. 2(b), (d)). Thus, the effect of these two fields simultaneously applied consists in a shift of the oscillation center and an electron density distribution of ellipsoidal shape. The ellipsoid becomes more elongated in the field direction as the QD radius and the magnetic field strength increase.
The presence of a hydrogenic impurity into the QD generates the appearance of an electric multipolar structure whose polarizability we calculate.

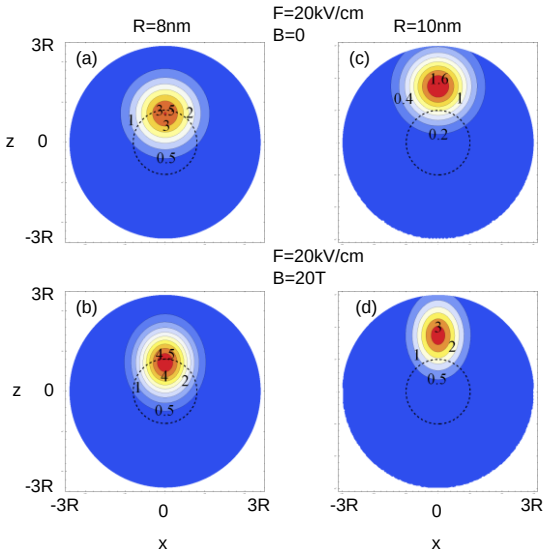

Fig. 2. (Color online) The cross section of the electron probability density for the ground level of spherical GaAs QD without impurity under different strengths of the applied electric and magnetic fields directed along the negative *z*-axis. The observation plane is *xOz*. The left panel is for R = 8 nm, and the right panel for R = 10 nm. The circles drawn with dashed line represent the QDs boundary.

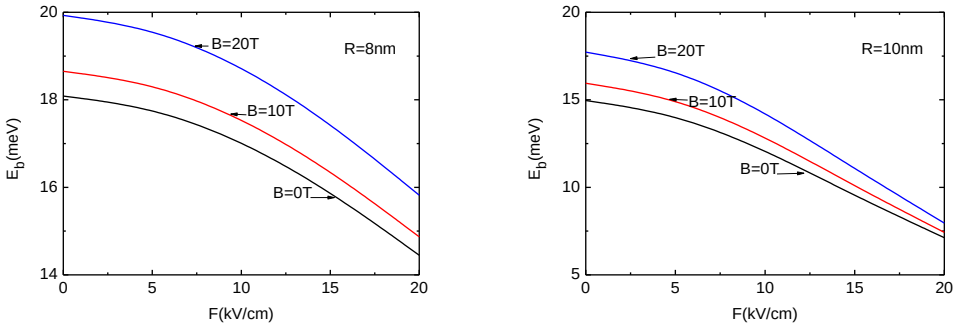

a) b)

Fig. 3. (Color online) The binding energy of the on-center donor impurity in spherical GaAs quantum dots with parabolic confinement, versus the applied electric field strength. The results are for two different spherical dot radii: (a) R=8nm and (b) R=10nm. Several values of the magnetic field strength are considered.

The Fig. 3 shows the dependence of the binding energy of the on-center impurity on the applied electric field strength for the same two already considered QD radii and several magnetic field values.

We note a decrease of the binding energy as the electric field strength increases and an increase of this quantity as the magnetic field value grows. This behavior can be explained by considering that the electric field may induce an enlarged dipole length while the magnetic field has contrary effect. Other authors [25, 26, 32] have also reported similar results.

The Figs. 4 and 5 show the same analysis given in Figs. 1 and 2 but in the presence of the impurity located at the center of QDs. The effects of the applied fields on the electron energy and distribution already shown generally remain the same in the presence of the impurity.

However there is a difference that worth to be highlighted. In both sections (z = 0 and y = 0 planes) there is an evident tendency of the electron cloud to stay near the impurity position. As result a notable difference from the Figs. 2 (b) and (d) appears: the density distribution takes the shape of an asymmetrical ellipsoid (a drop-like shape) with the sharp part directed toward impurity located in the QD center. In Figs. 5 (a) and (c) although the magnetic field is absent, we note a drop-like shape of the density distribution because the static electric field shifts the oscillation centre but the Coulomb interaction directed toward the impurity position opposes this trend.

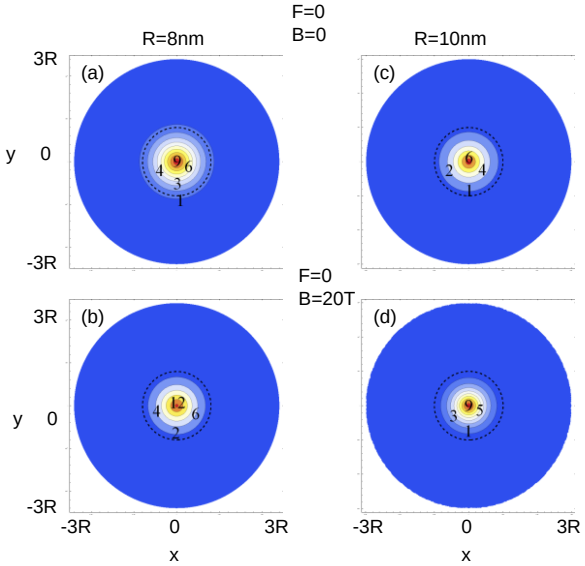

Fig. 4. (Color online) The cross section of the electron probability density for the ground level of spherical GaAs QD with on-center impurity under different strengths of the applied magnetic field directed along the negative z-axis. The observation plane is xOy. The left panel is for R = 8 nm, and the right panel for R = 10 nm. The circles drawn with dashed line represent the QDs boundary.

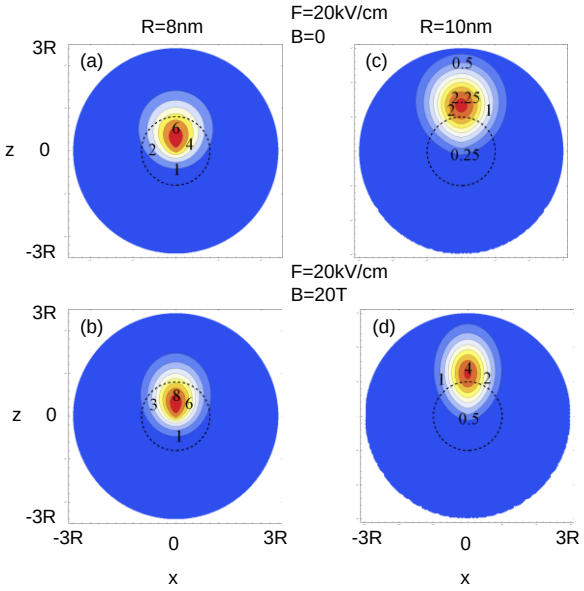

Fig. 5. (Color online) The cross section of the electron probability density for the ground level of spherical GaAs QD with on-center impurity under different applied electric and magnetic fields directed along the negative *z*-axis. The observation plane is *xOz*. The left panel is for R = 8 nm, and the right panel for R = 10 nm. The circles drawn with dashed line represent the QDs boundary.

The binding energy dependence on the impurity position inside the quantum dot is shown in the Fig. 6. The impurity position varies between -R and +R along the direction of applied fields for the dot radii $R = 8\,\text{nm}$ (the left panel) and $R = 10\,\text{nm}$ (the right panel). The magnetic field strength values are $B = 0, 10, 20\,\text{T}$ and the electric field strength values are $F = 0, 10, 20\,\text{kV/cm}$ marked by (a), (b), (c) respectively, on the curves.

The effects of the applied fields generally remain the same as in the discussed case of the on-center impurity when the impurity is located in $-R < z_i < 0$ domain, namely the binding energy monotonically decreases when electric field strength increases. For $F = 0$ it can be seen that the binding energy has the maximum value when the impurity is located on the dot center; the electric field presence leads to getting the binding energy maximum for other positions outside the dot center when the impurity location is in $0 < z_i < R$ domain.

In the on-center donor position case the polarizability due to the electron cloud versus the electric field strength both in the absence and presence of the magnetic field is plotted in Fig.7 for two dot radii. One can note that the polarizability increases as the QD radius and electric field strength increase while the opposite effect of the magnetic field is quite low.

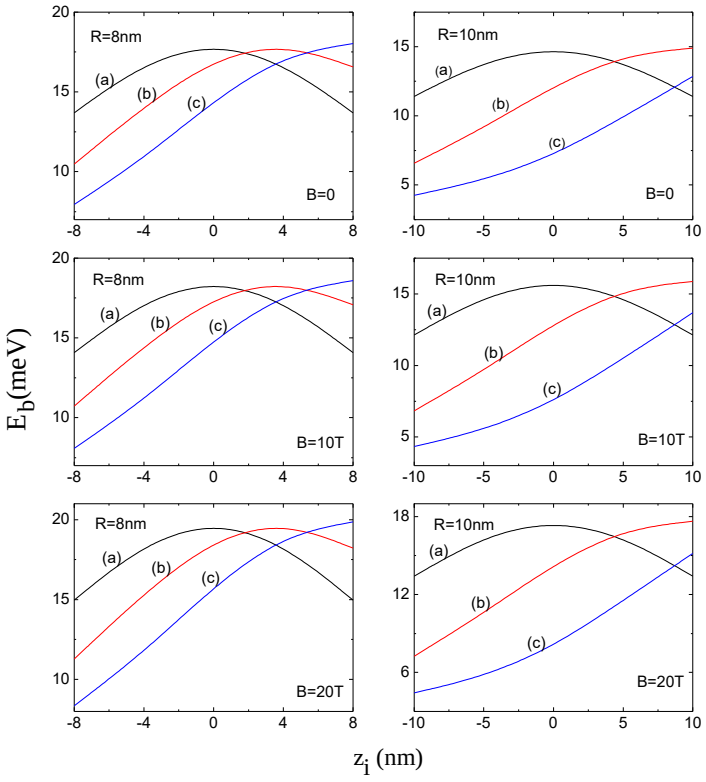

Fig. 6. (Color online) The binding energy versus the donor position z_i along the direction of applied fields for F = 0, 10, 20 kV/cm marked by (a), (b) and (c) respectively. The results are for two different spherical dot radii: R=8 nm (the left panel) and R=10 nm (the right panel). Several values of the magnetic field strength are considered.

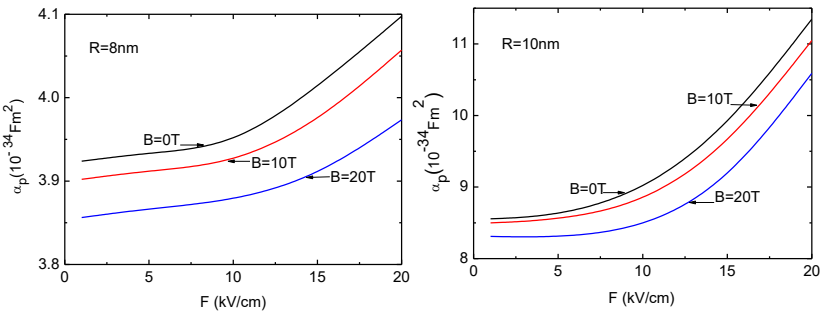

Fig. 7. (Color online) The polarizability versus the applied electric field strength for on-center donor impurity in spherical GaAs quantum dots with radial confinement. The results are for two different spherical dot radii: (a) R = 8 nm and (b) R = 10 nm and for three magnetic field strengths (B = 0, 10 T and 20 T).

When the impurity is on the quantum dot center in the absence of the applied electric field the electron cloud has a spherical symmetry due to elastic and Coulomb potentials and it is additionally confined around this position by the magnetic field. The applied electric field moves the electron cloud toward positive *z*-axis and as a result, the average value $\langle z \rangle$ and the polarizability increase.

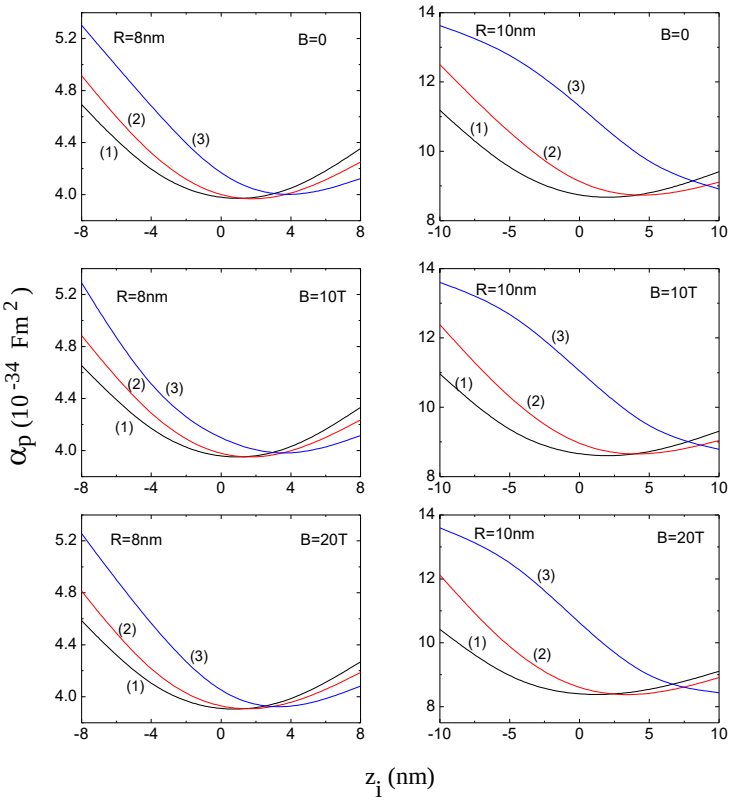

Fig. 8. (Color online) The polarizability versus the impurity position z_i along the direction of applied fields for F = 5, 10, 15 kV/cm marked by (1), (2) and (3) respectively. The results are for two different spherical dot radii: R = 8 nm (the left panel) and R = 10 nm (the right panel) and for three magnetic field strengths (B = 0, 10 T and 20 T).

The polarizability dependence on the impurity position along the direction of applied fields inside the quantum dot is shown in the Fig. 8 for different electric and magnetic strength values.

We firstly note that also in this case, the influence of the magnetic field on the polarizability values is very weak for the considered dot radii and magnetic field strengths.

The effect of the electric field on the polarizability is different if the impurity is displaced in the positive or negative way of the *z*-axis due to the distinct way of effect combination of the Coulomb field and applied electric field. The impurity

Coulomb field makes a deformation of the electron cloud when the impurity is displaced in any other position inside the quantum dot and $F = 0$.
For the negative z_i impurity positions the effect of the applied electric field is a monotonous increase of $\langle z \rangle$ values and polarizability. When impurity is closer to the dot center the cloud deformation is smaller and so is its polarizability.
The effect of the applied electric field on the electron cloud is slightly different for the positive z_i impurity positions. The change of the cloud average position values first decrease until the Coulomb field deformation effect is compensated by that of the increasing applied field; then, when the cloud center overpasses the impurity position, the $\langle z \rangle$ values increase again for higher F. Therefore, the polarizability curves show minimum values when the impurity position approximately coincides with the electron cloud center.

4. Conclusions

In summary, in the present work we have studied the effects of applied electric and magnetic fields on the donor impurity related polarizability in GaAs spherical quantum dots.
The behavior of the polarizability can be understood in terms of the localization properties of the electron cloud, properties that can be modified by the applied electric and magnetic fields and depending on the QD radius, too. The electric field shifts the electron oscillation center, reduces the electron-impurity pair binding energy and as result increases the polarizability. The magnetic field has the opposite effect: it induces an ellipsoidal symmetry that makes the mean electron-impurity distance to be shortened, increases the binding energy, resulting in smaller polarizability values. These applied field effects are more evident when the QD size is larger as it is expected.
Our results show that the polarizability values for the impurity fixed positions inside the quantum dots can be significantly controlled by the applied electric and magnetic field strengths.

REFERENCES

[1] *D.A. Cardimona, C.P. Morath, D.H. Guidry, V.M. Cowan*, Infrared Phys. Technol. **59**, 93 (2013).
[2] *N.N. Ledentsov*, Semicond. Sci. Technol. **26**, 014001 (2011).
[3] *Y.M. He, Y. He, Y.J. Wei, D. Wu, M. Atature, C. Schneider, S. Hofling, M. Kamp, C.Y. Lu, J.W. Pan*, Nat. Nanotechnol. **8**, 213 (2013).
[4] *T. Kambara, T. Kodera, Y. Arakawa, S. Oda*, Jpn. J. Appl. Phys. **52**, 04CJ01 (2013).
[5] *A.J. Nozik*, Physica E **14**, 115 (2002).
[6] *J. Brault, B. Damilano, A. Kahouli, S. Chenot, M. Leroux, B. Vinter, J. Massies*, J. Crys. Grouth **363**, 282 (2013).

[7] *Yuan Jian-Hui, Xie Wen-Fang, He Li-Li*, Commun. Theor. Phys. (Beijing, China) **52**, 710 (2009).
[8] *S. Wang, G. Wei, G. Yi*, Int. J. Mod. Phys. B **24**, 4293 (2010).
[9] *Jian-Hui Yuan, Chao Liu*, Phys. E **41**, 41 (2008).
[10] *C. Dane, H. Akbas, S. Minez, A. Guleroglu*, Phys. E **42**, 1901 (2010).
[11] *C.M. Duque, J.D. Correa, A.L. Morales, M.E. Mora-Ramos, C.A. Duque*, Phys. E **77**, 34 (2016).
[12] *J.D. Correa, M.E. Mora-Ramos, C.A. Duque*, Phys. B **472**, 25 (2015).
[13] *C.A. Duque, M.E. Mora-Ramos, J.D. Correa*, Superlatt. Microstruct. **87**, 25 (2015).
[14] *B. Çakir, Y. Yakar, A.Özmen*, J. Luminescence, **132** (10), 2659 (2012).
[15] *M.G.Barseghyan*, Phys. E **69**, 219 (2015).
[16] *J.G. Acosta, M.R. Joya, J. Barba-Ortega*, Int. J. Mod. Phys. B **29**, 1550228 (2015).
[17] *E. Kasapoglu, F. Ungan, H. Sari, I. Sökmen, M.E. Mora-Ramos, C.A. Duque*, Superlatt. Microstruct. **73**, 171 (2014).
[18] *B. Akbarnavaz Farkoush, G. Safarpour, M. Dialameh*, Superlatt. Microstruct. **63**, 149 (2013).
[19] *M.G. Barseghyan, H.M. Baghramyan, D. Laroze, J. Bragard, A.A. Kirakosyan*, Phys. E **74**, 421 (2015).
[20] *S.A.A. Kohl, R.L. Restrepo, M.E. Mora-Ramos, C.A. Duque*, Physica Status Solidi (B) Basic Research **252** (4), 786 (2015).
[21] *A. Tiutiunnyk, V. Tulupenko, M.E. Mora-Ramos, E. Kasapoglu, F. Ungan, H. Sari, I. Sökmen, C.A. Duque*, Phys. E **60**, 127 (2014).
[22] *J.C. Martínez-Orozco, M.E. Mora-Ramos, C.A. Duque*, Phys. B **452**, 82 (2014).
[23] *G.V.B. deSouza, A.Bruno-Alfonso*, Phys. E **66**, 128 (2015).
[24] *H. Bahramiyan, R. Khordad*, Int. J. Mod. Phys. B **28**, 1450053 (2014).
[25] *A.L. Morales, N. Raigoza, E. Reyes-Gomez, L.M. Osorio-Guillen, C.A. Duque*, Superlatt. Microstruct. **45**, 590 (2009).
[26] *A.J. Peter*, Superlatt. Microstruct. **44**, 106 (2008).
[27] *A.J. Peter*, Phys.Lett. A **355**, 59 (2006).
[28] *E. Tangarife, C.A. Duque*, Applied Surface Science **256,** 7234 (2010).
[29] *E. Tangarife, C.A. Duque*, Phys. B **406**, 952 (2011).
[30] *R. Khordad, A. Gharaati, M. Haghparast*, Current Applied Physics **10**, 199 (2010).
[31] *M. Cristea, E.C. Niculescu*, Superlatt. Microstruct. **62**, 269 (2013).
[32] *H. Satori, A. Sali, M. Fliyou, A. Nougaoui*, Phys. Low-Dim. Struct. **7/8**, 141 (2001).
[33] *A.R. Jeice, S.G. Jayams, K.S.J. Wilson*, Chin. Phys. B **24**, 110303 (2015).
[34] *M.E. Mora-Ramos, M.G. Barseghyan, C.A. Duque*, Phys.Status Solidi B **248**, 1412 (2011).
[35] *Z. Zeng, C.S. Garoufalis, S. Baskoutas*, J. Phys. D: Appl. Phys. 45, 235102 (2012).
[36] *Z. Zeng, G. Gorgolis, C.S. Garoufalis, S. Baskoutas*, Sci. Adv. Mater. 6, 586 (2014).
[37] *A. Bera, M. Ghosh*, J. Alloys Compd. 695, 3054 (2017).
[38] *A. Ghosh, A. Bera, M. Ghosh*, Biointerface Research in Appl. Chem. 6, 1573 (2016).
[39] *M.S. Atoyan, E.M. Kazaryan, H.A. Sarkisyan*, Phys. E **31**, 83 (2006).
[40] *B. Li, K.X. Guo, Z.L. Liu, Y.B. Zheng*, Phys. Lett. A **372**, 1337 (2008).
[41] *L.M. Burileanu, E.C. Niculescu, N. Eseanu, A. Radu*, Phys. E **41**, 856 (2009).
[42] M.G. Barseghyan, A.A. Kirakosyan, C.A. Duque, Eur. Phys. J. B **72**, 521 (2009).